ACS APPLIED POLYMER MATERIALS

pubs.acs.org/acsapm Article

Stereolithography 3D Printing of Microcapsule Catalyst-Based Self-Healing Composites

Vinita V. Shinde, Asha-Dee Celestine, Lauren E. Beckingham, and Bryan S. Beckingham*

Cite This: *ACS Appl. Polym. Mater.* 2020, 2, 5048−5057 Read Online

ACCESS | Metrics & More | Article Recommendations | Supporting Information

ABSTRACT: Polymer-based components manufactured by stereolithography-based (SLA) three-dimensional (3D) printing tend to show relatively poor mechanical strength compared to polymer-based components fabricated by conventional methods such as compression molding. Some of this difference is related to the thermoset nature of typical SLA 3D-printed materials, where high cross-linking density and brittle material behavior can result in catastrophic material failure, limiting the life span of SLA 3D-printed composite materials. Previous studies have investigated potential techniques for improving the mechanical strength of SLA 3D-printed polymer components, such as the addition of various strengthening fillers; however, a few studies have investigated the incorporation of self-healing materials for SLA 3D printing to extend material lifetimes. In this study, we investigate the use of a microcapsule catalyst self-healing system in conjunction with commercially available photocurable resin toward increasing SLA 3D-printed specimen lifetime and material sustainability. Microcapsules filled with healing fluids are synthesized using in situ interfacial polymerization and dispersed in commercial resin prior to SLA 3D printing of self-healing composite specimens. The ability of these microcapsules to survive the SLA 3D printing process intact is demonstrated, and X-ray nano-computed tomography (X-ray Nano-CT) imaging shows microcapsules to be distributed throughout printed specimens. The self-healing behavior of these SLA 3D-printed composite materials is evaluated via quantification of mechanical properties, and healing efficiency. Overall, this is a facile and promising approach for the incorporation of self-healing behavior into SLA 3D printing resins.

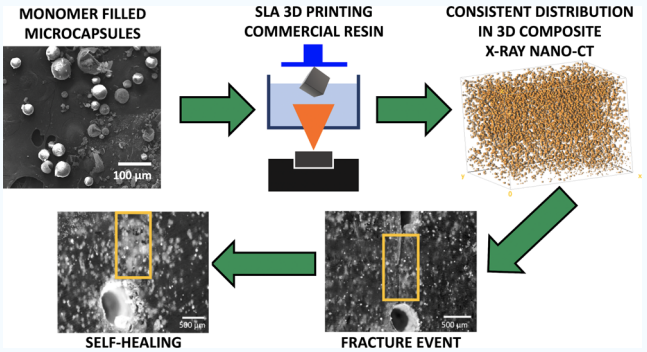

KEYWORDS: *3D printing, stereolithography, microcapsules, self-healing composites, healing efficiency*

Downloaded via AUBURN UNIV on July 20, 2021 at 16:26:02 (UTC).
See https://pubs.acs.org/sharingguidelines for options on how to legitimately share published articles.

1. INTRODUCTION

Stereolithographic three-dimensional (SLA 3D) printing of thermoset polymers for industrial applications has been rapidly evolving over the last decade.[1−5] The expansion of interest is driven by its high degree of customization, ability to construct complex designs with high precision, and excellent surface finish.[6,7] SLA 3D printing builds an object layer by layer using photopolymerization. During SLA, a beam of light is focused to a spot within a liquid resin bath, activating a photoinitiator that begins the polymerization process. By controlling the light position and resin chemistry, desired objects are printed from this liquid resin bath into the final solid object; the objects' architectures are manipulated utilizing a variety of computer-aided design (CAD) programs.[8] Cross-linking of 3D-printed structures leads to various properties including high glass-transition temperature, high modulus, good solvent resistance, and high tensile strength.[9] In conjunction with the increasing ease and accessibility of 3D printing processes, the interplay of these properties has led to an extensive use of 3D printing of thermoset resins for rapid prototyping for industrial applications and as matrix materials for reinforced composites. However, 3D printing of thermoset polymer materials remains constrained by limitations in mechanical properties and functionalities afforded by the various SLA resin chemistries compared to traditionally constructed components.[6,7] The cross-linked nature of SLA-printed specimens leads to relatively low toughness and elongation, resulting in brittle fracture and catastrophic material failure, which, combined with poor resistance to crack initiation, limit the useful life of these SLA 3D-printed materials.[10−12]

Additionally, many options for 3D printing of thermoset polymer materials are not intrinsically sustainable or recyclable due to their cross-linked networks requiring disposal if they suffer any damage during processing or use. In nature, biological systems overcome this issue by using self-healing

Received: August 11, 2020
Accepted: October 2, 2020
Published: October 19, 2020

ACS Publications © 2020 American Chemical Society

https://dx.doi.org/10.1021/acsapm.0c00872
ACS Appl. Polym. Mater. 2020, 2, 5048−5057

as their survival strategy to heal injuries.[13] Thus, taking inspiration from nature, we investigate the fabrication of self-healing thermoset composites using SLA 3D printing to extend material lifetimes. Self-healing materials can be categorized as either intrinsic or extrinsic.[14,15] Intrinsic self-healing materials repair damage using latent functionality of a polymer material and recover the material's properties by reversible polymerization, hydrogen bonding, or molecular diffusion and typically requires an external trigger to initiate the healing.[16−19] Extrinsic self-healing materials repair their damage without external intervention using embedded healing materials in the form of microcapsules or vascular capillaries containing healing fluids.[20−23] During the fracture event, healing fluid releases into the damage site and seals the crack by polymerization or entanglement process.[24] As intrinsic self-healing systems work on the principle of molecular diffusion, they are typically limited to thermoplastic materials and elastomers.[21] However, in the case of microcapsule-based self-healing, thermoset polymers can also be used, as molecular diffusion of polymer chains is not a requirement for healing.[19] In 2001, White et al. showed for the first time autonomous, extrinsic, microcapsule-based self-healing by embedding Grubbs' catalyst particles and dicyclopentadiene (DCPD)-filled microcapsules into an epoxy matrix.[21] When microcapsules are ruptured, DCPD fluid releases to the crack location, and with the help of a catalyst, it forms cross-linked networks around the crack plane, healing the fracture and restoring mechanical integrity of thermoset materials.[21] Since that first demonstration, several studies have explored different encapsulation chemistries in microcapsule synthesis and their capability of healing fractures within polymer matrices or at the polymer−fiber interface in composites.[20,21,25−32]

Recently, coupled with the increasing interest in the 3D printing technology, there has been increasing attention paid to improving material properties and incorporating functionalities developed for traditional composites into 3D printing platforms.[33,34] Studies on 3D printing of self-healing thermoset polymer composites have only recently been reported.[24,35−37] For instance, Yu et al. included self-healing properties in elastomers by incorporating thiol and disulfide groups within the structure, which undergo reversible reactions enabling healing.[37] Also, direct 3D printing of hydrogels for developing strain sensors for wide applications in health monitors, sports, and electronic skin has been reported.[38−41] However, these reports typically use intrinsic physical and chemical properties of the matrix polymer or external trigger such as heat to initiate self-healing.[37,38] In addition, in 2019, Sanders et al. reported on the self-healing of stereolithographic 3D-printed thermoset composites using anisole (solvent)-filled microcapsules to enable self-healing upon microcapsule rupture, a solvent welding mechanism.[24] Using this route, a healing efficiency (ratio of fracture toughness of healed material to that of the virgin material) of 87% was achieved after 3 days.[24] However, this route is dependent on the solubility of matrix resin in the solvent. The use of solvent healing cannot be generalized for all resin materials as the requisite solvent characteristics for each resin material will vary based on their solubility parameter. Moreover, the presence of solvent can soften the polymer matrix after the healing process.[25,42−44] These drawbacks can be overcome using a microcapsule catalyst system, the focus of this work, where healing requires a dispersed catalyst for polymerization of an encapsulated monomer (healing fluid) to provide self-healing in response to a damage event. In addition, such microcapsule catalyst systems can be used for a wide variety of thermoset resins as it is essentially independent of the matrix material chemistry.

Herein, we demonstrate stereolithographic (SLA) 3D printing of a self-healing composite system consisting of a commercial photocurable resin with embedded catalyst (Grubbs') and microcapsules containing dicyclopentadiene (DCPD) monomer. The mechanism of this system relies on monomer (DCPD) release at the fracture site and its subsequent room temperature catalytic polymerization to restore the mechanical properties and local structural integrity of the surrounding polymer matrix. This autonomous self-healing mechanism of microcracks within 3D-printed composite structures can enable retention of material matrix integrity toward preventing or delaying mechanical failure of SLA 3D-printed materials. Microcapsule survivability after SLA 3D printing is demonstrated using ^{1}H nuclear magnetic resonance (NMR) spectroscopy. Microcapsule dispersion in the polymer matrix and response to induced fracture and fracture sealing is characterized using optical microscopy, scanning electron microscopy (SEM), and 3D X-ray nano-computed tomography (CT). The self-healing behavior of these 3D-printed composite structures is investigated using single-edge notch bend (SENB) tests, demonstrating recovery of material's fracture toughness over 72 h. Overall, this investigation demonstrates that SLA 3D-printed self-healing composites based on microcapsule catalyst autonomous self-healing are a promising and flexible approach for fabricating 3D objects with self-healing characteristics.

2. EXPERIMENTAL METHODS

2.1. Materials. All chemicals and solvents were used as received unless otherwise noted. First-generation Grubbs' catalyst and ethyl phenylacetate (EPA) were purchased from Sigma-Aldrich. Polyurethane (PU) prepolymer (Desmodur L 75) was graciously donated by Covestro. Desmodur L 75 is a prepolymer solution in ethyl acetate with a reported equivalent weight of 315 g and an isocyanate content of 13.3 ± 0.4 wt %. Ethylene-maleic anhydride (EMA) copolymer (Zemac-400) powder was purchased from Polyscience, Inc. and used as a 2.5 wt % aqueous solution. Dichloromethane, urea, ammonium chloride (NH_4Cl), and sodium hydroxide (NaOH) pellets were purchased from BDH chemicals. NaOH (0.5 N) and hydrochloric acid solution (0.5 M) were prepared and used to adjust the pH of the emulsion. Formaldehyde solution (formalin, 37 w/v %) was purchased from BTC Chemicals. Dicyclopentadiene (DCPD) and hydrochloric acid (95% purity) were purchased from Merck Chemicals. 1-Octanol was purchased from Fischer Chemicals. Anycubic SLA UV curing resin was purchased from Shenzhen ANYCUBIC Technology Co., Ltd. Isopropanol and acetone were purchased from VWR. Deuterated chloroform ($CDCl_3$) was purchased from EMD Millipore. All solvents and chemicals used for the preparation of EMA solution, acid and base solutions, and 1-octanol were of analytical grade.

2.2. Preparation of PU/UF Microcapsules with DCPD Core Fluid. Double-walled microcapsules were synthesized following the general procedure of Caruso et al.,[22] which synthesizes polyurethane/poly(urea-formaldehyde) (PU−UF) microcapsules in a single batch process. The procedure combines in situ poly(urea-formaldehyde) microencapsulation with an interfacial microencapsulation using a PU prepolymer (Desmodur L 75).[22] Briefly, 2.5 wt % poly(ethylene-*alt*-maleic anhydride), EMA, in water was prepared by adding 3.75 g of EMA to 150 mL of water and allowing to stir for 24 h. This 2.5 wt % aqueous solution of EMA copolymer (50 mL) and deionized water (200 mL) were blended at 550 rpm with a magnetic stirrer in a 500 mL beaker placed in a temperature-controlled water bath (25 °C). Under blending, 5.00 g of urea, 0.50 g of ammonium chloride, and

https://dx.doi.org/10.1021/acsapm.0c00872
ACS Appl. Polym. Mater. 2020, 2, 5048−5057

0.50 g of resorcinol were added sequentially to the previous solution. The pH was increased from ~2.60 to 3.50 by dropwise addition of 0.5 N sodium hydroxide solution. One to two drops of 1-octanol were then added to expel surface air bubbles. Separately, 3 g of Desmodur L 75 was dissolved in 20 mL of dichloromethane in a water bath maintained at 80 °C. Subsequently, 60 mL of dicyclopentadiene DCPD was slowly added to this solution, and the solution was stirred continuously for an hour before adding to the above-described aqueous solution to form an emulsion under stirring for 10−20 min. Once stabilized, 12.67 g of 37 wt % aqueous solution of formaldehyde was added to achieve a 1:1.9 molar proportion of formaldehyde to urea. The emulsion was covered with aluminum foil and heated to 55 °C with continuous mixing at 600−800 rpm. Following 4 h of mixing, the hot plate was turned off and the solution was cooled to room temperature. Microcapsules were then captured from the suspension with a coarse-fritted funnel under vacuum, washed with deionized water, and air-dried for 24−48 h. After drying, microcapsules were sieved using a stack of laboratory sieve trays with mesh sizes of 90, 106, 150, and 212 μm under mechanical shaking to isolate fractions of the synthesized microcapsule size distribution. A batch of EPA-containing microcapsules was also prepared using an analogous procedure for inclusion in SLA 3D-printed specimens for X-ray Nano-CT characterization to ensure microcapsule stability during shipping and handling; details are given below.

2.3. Characterization of Neat Microcapsules. Optical microscope images of microcapsules were captured using an OLYMPUS 52 × 7 optical microscope at varied magnifications and analyzed for microcapsule diameter (175 microcapsules) using ImageJ. Thermogravimetric analysis (TGA) was carried out on a TA Instruments Q500 equipped with an autosampler to evaluate the thermal stability of the microcapsules. TGA samples were heated at a rate 10 °C/min from 25 to 600 °C under nitrogen flow.

2.4. SLA 3D Printing of Microcapsule-Containing Composites. Double-walled DCPD microcapsules of average diameter 96 ± 11 μm were used to probe microcapsule-composite material self-healing capabilities. Formulations of microcapsules (5 wt %) in commercial ANYCUBIC resin were prepared by addition of the microcapsules and 0.5 wt % of first-generation Grubbs' catalyst to the resin, followed by mixing the dispersion at 500−600 rpm for 10−15 min to distribute the microcapsules and catalyst in the resin. The mixture was poured into the resin tank of an ANYCUBIC SLA printer, and an STL file of a desired 3D structure was loaded into the ANYCUBIC Photon Slice64 software, provided by ANYCUBIC to generate a photon file, and a layer height of 100 μm was selected. Finished prints were immediately washed with isopropyl alcohol to remove uncured resin on the outer surface of the specimen, and the sample was placed under a UV lamp for 3−5 min for finishing. Rectangular composite bars of dimensions 52.8 × 12 × 6 mm^3 were 3D-printed and used for mechanical testing, SEM, and confirmation of microcapsules surviving the printing process. Solid cubes (20 × 20 × 20 mm^3) and cubical grid lattices (15 × 15 × 15 mm^3) were 3D-printed with and without EPA-containing microcapsules and used for X-ray Nano-CT characterization; the details are given below.

2.5. Characterization of 3D-Printed Self-Healing Composites. *2.5.1. ^{1}H Nuclear Magnetic Spectroscopy.* The survivability of the microcapsules in SLA 3D-printed composite specimens was evaluated through the release of the core healing fluid (DCPD) after mechanically crushing specimens. Fabricated SLA 3D-printed specimens containing 5 wt % microcapsules and 0.5 wt % catalyst were physically crushed and rinsed with $CDCl_3$. The $CDCl_3$ rinse was filtered to remove SLA resin debris and catalyst. The filtrate was loaded into an NMR tube and characterized using low-field (60 MHz) ^{1}H NMR spectroscopy. ^{1}H-NMR spectra were collected on an Oxford Instruments Pulsar 60 MHz spectrometer.

2.5.2. Scanning Electron Microscopy. Scanning electron microscopy (SEM) was performed using a Zeiss EVO50 SEM to visualize the fracture plane of an SLA-printed composite containing monomer-filled microcapsules. The fracture surface was obtained by cutting the specimen with a Buehler Isomet 1000 precision cutter and washing with isopropyl alcohol to remove any residual DCPD monomer released by microcapsule rupture. Cut specimens were then sputter-coated with gold using an EMS 550X Auto Sputter Coating Device with carbon coating attachment prior to analysis.

2.5.3. X-ray Nano-CT. X-ray Nano-CT is a nondestructive technique to visualize the inner morphology of materials. Here, X-ray Nano-CT is used to visualize the presence and distribution of microcapsules within 3D-printed composites. X-ray Nano-CT images of square samples (2 × 2 × 2 cm^3) printed with and without 5 wt % EPA-containing microcapsules with a mean diameter and standard deviation (determined by optical imaging analysis) of 129 ± 16 μm were obtained at the University of Florida Research Service Center with a Nano-CT-GE V/TOME/X M 240 with an image resolution of 21.4 μm. The acquired images of the solid square cubes were segmented into microcapsule and matrix polymer voxels by intensity using MATLAB, where the threshold was determined manually in ImageJ. The image stack was then converted into a 3D binary image, and the properties of the microcapsules were analyzed using bwconncomp in MATLAB to determine the volume and centroid location of clusters larger than 70 μm diameter. The diameter of the identified microcapsules was determined assuming a spherical geometry of microcapsules. X-ray Nano-CT of cubical grid lattice structures (15 × 15 × 15 mm^3) with and without analogous 5 wt % EPA-containing microcapsules were obtained using a Zeiss 620 Versa located at Auburn University with an image resolution of 22.2 μm. The brightness of cubical grid lattice images was adjusted for clarity and examined for microcapsule presence and general features.

2.5.4. Dynamic Mechanical Analysis. The thermomechanical behavior of the SLA 3D-printed self-healing composites was characterized by dynamic mechanical analysis (DMA) using a TA Instruments RSA III DMA. Storage modulus (E') at room temperature and glass-transition temperature (T_g, extracted as the peak in tan delta) of 3D-printed SLA composites was determined using a dynamic temperature ramp test with a frequency of 1 Hz and heat rate of 5 °C/min.

2.5.5. Fracture Toughness. Single-edged notched beam (SENB) (ASTM D5045-14) testing was used to evaluate fracture toughness and the self-healing efficiency of microcapsule-loaded SLA 3D-printed composites.[44,45] The self-healing efficiency of a material is defined as a ratio of the fracture toughness, K_Q, of the healed material to that of the virgin material (eq 1).

$$\text{healing efficiency} = \frac{K_{Q(\text{healed})}}{K_{Q(\text{virgin})}} \tag{1}$$

Displacement-controlled SENB tests were performed using a screw-driven Instron mechanical test frame (Model Instron 5565) with a 5 kN load cell at a loading rate of 5 mm/min. Specimens of dimensions 52.8 × 12 × 6 mm^3 with a preinduced notch and a natural crack were used. An initial crack length of 6 mm was used corresponding to an approximate a/W value of 0.5, where a is the length of the crack and W is the width of the specimen. The value of $f(x)$ is then calculated using eq 2

$$f(x) = 6x^{1/2}\frac{[1.99 - x(1-x)(2.15 - 3.93 + 2.7x^2)]}{(1+2x)(1-x)^{3/2}} \tag{2}$$

where x is the a/W value. Fracture toughness (K_Q) of the specimen was calculated using eq 3

$$K_Q = \left(\frac{P_Q}{BW^{1/2}}\right) f(x) \tag{3}$$

where K_Q is the fracture toughness, P_Q is the offset intercept, B is the specimen thickness, and W is the specimen width. The value of P_Q for each specimen is obtained from the load versus extension plot using a 5% reciprocal slope offset.

3. RESULT AND DISCUSSION

3.1. Synthesis and Characterization of PU−UF Double-Walled Microcapsules. Double-walled microcap-

https://dx.doi.org/10.1021/acsapm.0c00872
ACS Appl. Polym. Mater. 2020, 2, 5048−5057

sules with DCPD as a core fluid were synthesized by in situ interfacial polymerization due to their thicker and more robust shell walls compared to single-walled microcapsules.[26,27,47,48] This is important for obtaining long-term microcapsule stability at elevated temperatures and high shear stress environments such as those in the processing of polymer materials and composites for additive manufacturing. This process successfully synthesized intact microcapsules with encapsulated healing fluid (DCPD). Optical microscope images of as-prepared microcapsules (Figure 1A) and subsequently crushed microcapsules (Figure 1B) are shown in Figure 1, where the presence of healing fluid is confirmed by its release upon microcapsule compression.

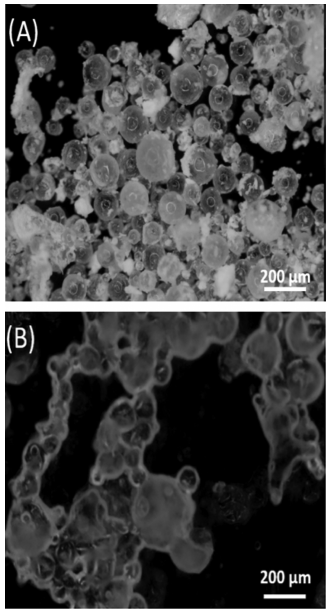

Figure 1. Optical microscopy image showing (A) spherical microcapsules and (B) microcapsules ruptured under the coverslip showing release of healing fluid.

TGA was performed on neat DCPD-containing microcapsules (Figure 2) for a heating cycle from 25 to 600 °C to evaluate the microcapsule thermal stability and verify the presence of DCPD core fluid after encapsulation. As shown in Figure 2, a dramatic loss in microcapsule weight is observed above 200 °C; a 5% weight loss occurs at 163 °C. We attribute this weight loss to microcapsule rupture and loss of DCPD as vapor at and above the normal boiling point of DCPD (170 °C).[16] As DCPD vaporizes, the rapid volumetric expansion causes the microcapsules to rupture. The appearance of this large drop at the DCPD boiling point is thereby a useful means of confirming that microcapsules contain the core healing fluid. Conversely, this is also an apt demonstration of how the boiling point of the healing fluid (here DCPD) is a limiting factor for the thermal stability of microcapsules for self-healing.

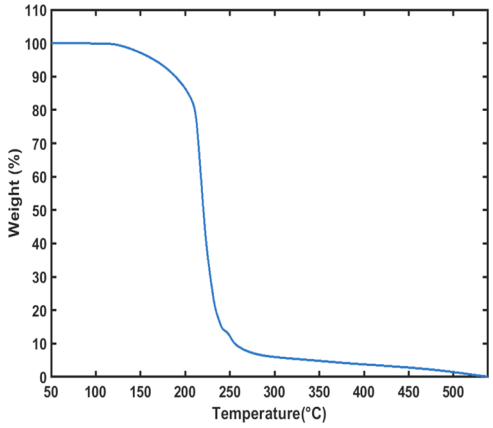

Figure 2. Representative TGA curve for PU/UF DCPD microcapsules.

Microcapsule size distribution was evaluated through optical microscopy (Figure 3). A total of 175 randomly selected microcapsules were chosen and measured yielding a mean microcapsule diameter of 82 ± 17 μm for the as-synthesized microcapsule batch. The particle size distribution of the as-synthesized microcapsules is quite broad with microcapsule diameter varying from 50 to 130 μm (Figure 3b). As described in Section 2, this microcapsule batch was then sieved, and the microcapsules captured on a 90 μm tray (and below a 106 μm tray) were used for subsequent work in this study; an optical image of sieved microcapsules is shown in Figure 3C. The size distribution of the sieved microcapsule batch was similarly quantified (Figure 3D) and was found to have an average diameter of 96 ± 11 μm. In Table 1, particle size distributions of the DCPD-containing microcapsules (as-synthesized as well as sieved) and EPA-containing microcapsules used in this work are shown. EPA-containing microcapsules were used for the X-ray Nano-CT characterization; see the Supporting Information for additional details on EPA-containing microcapsules.

3.2. Microcapsule Survivability in SLA-Printed Composites. *3.2.1. ^{1}H NMR Spectroscopy.* Existence of unbroken microcapsules in SLA 3D-printed composites was evaluated through the presence of DCPD in crushed composite specimens (52.8 × 12 × 6 mm^3) containing 5 wt % sieved double-walled DCPD microcapsules and 0.5 wt % catalyst. The crushed SLA 3D-printed specimens were rinsed with $CDCl_3$, the rinse was filtered, and the filtrate was analyzed by ^{1}H-NMR spectroscopy (Figure 4). The ^{1}H-NMR spectra in Figure 4 clearly show the presence of DCPD as the two expected distinct allylic peaks at 5.49 and 5.98 ppm appear in the area ratio of 1:1. Several peaks in the aliphatic region in the range of 1.3−3.21 ppm are also observed, which also correspond to DCPD; allylic protons at 5.49 and 5.98 ppm. This process demonstrates the presence of intact DCPD-filled microcapsules in the SLA 3D-printed specimen.

3.2.2. Scanning Electron Microscopy. The internal morphology of the SLA 3D-printed self-healing composites was examined with scanning electron microscopy (SEM). The fracture plane (Figure 5) shows spherical voids of various sizes where microcapsules were present within the material prior to fracture. These voids are within the range of microcapsule diameters present in the specimen, where we note that the different sizes of the voids are due to the two-dimensional (2D) fracture plane representing a projection through different slices of the spherical microcapsules present in the 3D structure prior to fracture.[49,50] The SEM image in Figure 5 also shows features in the fracture plane creating a tail-like appearance in the wake of the spherical voids. These tail markings originating from the voids have been previously attributed to the arresting of crack growth by the microcapsules, followed by rapid advancement of the crack front from the microcapsule−matrix interface.[51]

https://dx.doi.org/10.1021/acsapm.0c00872
ACS Appl. Polym. Mater. 2020, 2, 5048−5057

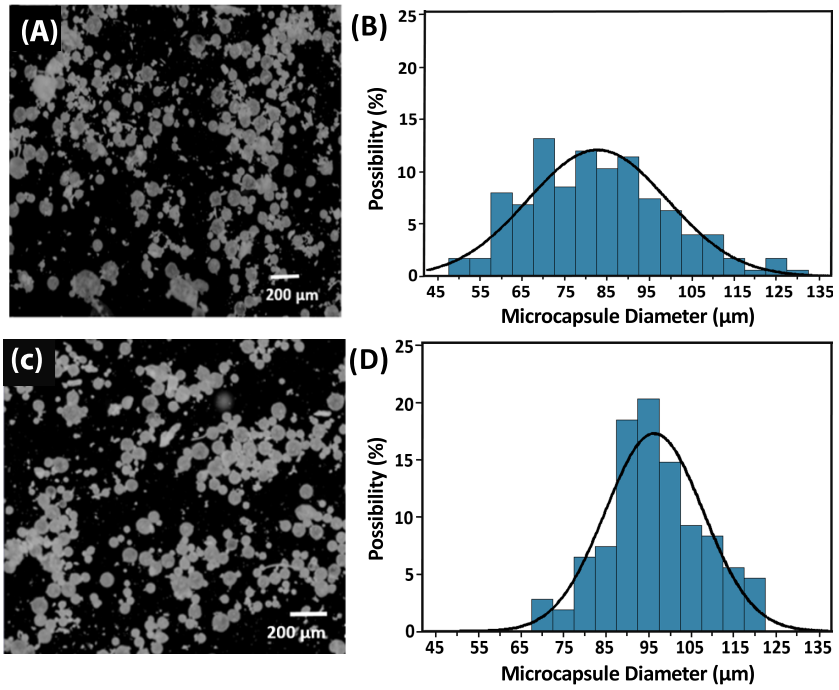

Figure 3. (A) Optical microscopy image of PU−UF (DCPD core) unsieved microcapsules and their (B) particle size distribution (mean diameter and standard deviation: 82 ± 17 μm). (C) Optical microscopy image of sieved PU−UF (DCPD core) microcapsules and (D) their particle size distribution (mean diameter and standard deviation: 96 ± 11 μm).

Table 1. Particle Size Distribution of Microcapsules

microcapsules	core fluid	mean capsule diameter (μm)	standard deviation (μm)
as-synthesized	DCPD	82	17
sieved	DCPD	96	11
as-synthesized	EPA	129	16

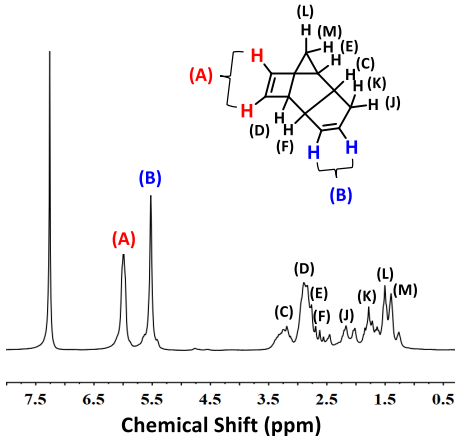

Figure 4. ^{1}H NMR spectra of DCPD extracted from SLA 3D-printed composite.

3.2.3. X-ray Nano-CT. The presence of microcapsules in the 3D-printed part was also examined using X-ray Nano-CT by examining the 3D image stack and 2D cross sections of the 3D image (Figure 6B,C, respectively). The particle size distribution frequency (number basis) of the microcapsules is extracted and shown in Figure 6D. The microcapsule size distribution could also be determined from the 3D image stack and was relatively broad, with 70% of microcapsules being 100−120 μm in diameter, and a mean diameter of 114 ± 25 μm. Overall, this microcapsule size distribution is in good agreement with that obtained from optical microscopy (mean diameter, 129 ± 16 μm); see the Supporting Information (Figure S1). A heatmap of the microcapsule centroid locations within the 3D-printed cube is shown in Figure 6F and gives a generalized view of the microcapsule size distributions within 12.5 μm thick horizontal cross sections of the 3D object. In this heatmap, a higher frequency of microcapsules is indicated by the color scale (blue to yellow—dark to light—for low to high microcapsule count). Microcapsules of diameter 100−130 μm show the highest proportion though a majority of the specimen. This is expected as these are the most abundant microcapsules in the size distribution. The cumulative microcapsule probability distribution on a volume basis extracted from the centroid analysis is shown in Figure 6E. In this volume-weighted distribution, the contribution of each microcapsule relates to its volume such that it is a good proxy for the quantity of healing fluid throughout the specimen. The obtained cumulative volume distribution curve generally tracks with a linear increase (shown via the solid blue line) along the vertical axis of the specimen. This indicates a relatively uniform

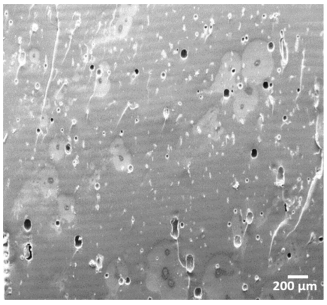

Figure 5. SEM image of self-healing composite showing spherical microcapsule voids.

https://dx.doi.org/10.1021/acsapm.0c00872
ACS Appl. Polym. Mater. 2020, 2, 5048−5057

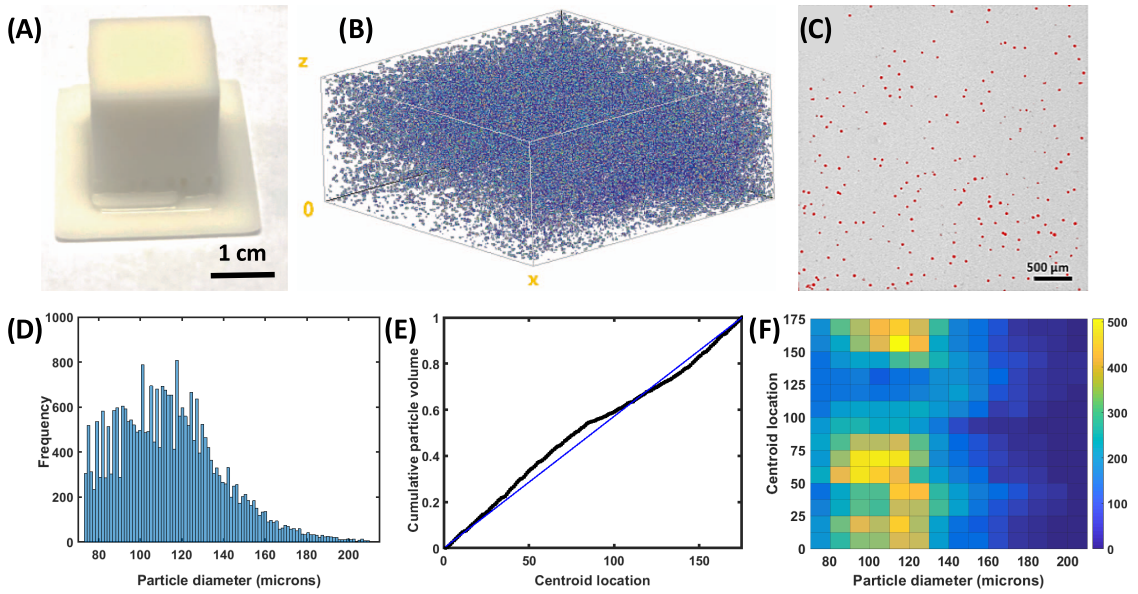

Figure 6. Visualization of X-ray Nano-CT data of SLA 3D-printed composites: (A) image of SLA 3D-printed composite containing EPA-filled microcapsules, (B) 3D visualization of microcapsules (colored) within the specimen (transparent) from X-ray Nano-CT data, (C) $x-y$ cross section of 3D Nano-CT image, (D) size frequency distribution of microcapsules, (E) (black line) cumulative particle distribution on volume basis for microcapsules located at the geometric center of 3D-printed composite, and (blue line) a linear cumulative particle volume vs centroid location fit corresponding to a uniform volume distribution, and (F) heatmap of microcapsules from blue to yellow (dark to light) for low to high microcapsule count.

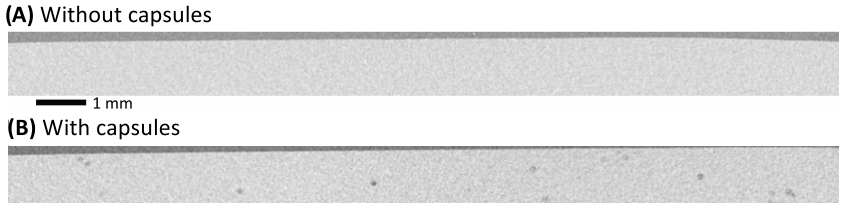

Figure 7. X-ray Nano-CT image of the edge of SLA 3D-printed specimens (A) without microcapsules and (B) with microcapsules.

distribution of microcapsule volume within the specimen and thereby a relatively uniform probability that a given random fracture would interact with microcapsules and thereby lead to localized self-healing.

Another consideration is the impact of microcapsules on surface features of the 3D-printed specimens. Here, we examine the surface using the edge as visualized in each 2D $x-y$ cross section of the X-ray Nano-CT data. The representative images of the edge plane for specimens with and without capsules are shown in Figure 7. These images show an edge of the cubes (light gray) with the surrounding air (dark gray) for a single slice through the sample for comparison. Overall, we found little difference in the surfaces and the surface variation for both was generally within the voxel resolution of the images. To examine the surface across the entire sample, the cross-sectional images were compiled into short videos scanning through the samples both with and without microcapsules; see the Supporting Information for videos.

To interrogate the impact of microcapsules on finer features, specimens with more complex geometry, a square lattice grid structure containing internal voids, were printed with and without 5 wt % EPA-containing microcapsules (see the photograph in Figure 8). The specimen with microcapsules was printed into the desired structure without any change in printing parameters, confirming the ability to print more complex features containing microcapsules. A set of 3D X-ray Nano-CT images of each sample were obtained to visualize the microcapsules within the structure and qualitatively compare the printed structures (Figure 8). Microcapsules are clearly evident in the specimen printed from the microcapsule-loaded resin and appear to be generally dispersed throughout the specimen. Here, we do note some visible differences between the surface structures between the specimens with and without microcapsules. The specimen printed with microcapsules appears to show additional defects compared to the specimen printed without microcapsules. Overall, this demonstrates the ability to incorporate microcapsules readily into complex geometries, but additional optimization of printing parameters as well as the microcapsule size and loading are necessary to ensure geometric integrity, if necessary, for more intricate structures with smaller geometric features in the printed specimens.

3.3. Physical Properties of SLA 3D-Printed Composites. *3.3.1. Dynamic Mechanical Analysis of SLA-Printed Composites.* The effect of the addition of microcapsules and catalyst on the storage modulus (E') and the glass-transition temperature (T_g) of SLA-printed composites was evaluated using dynamic mechanical analysis (DMA); see the Supporting Information for representative DMA data. As shown in Table 2, the addition of microcapsules slightly lowers E', while T_g remained essentially unchanged. To investigate the extent of

https://dx.doi.org/10.1021/acsapm.0c00872
ACS Appl. Polym. Mater. 2020, 2, 5048−5057

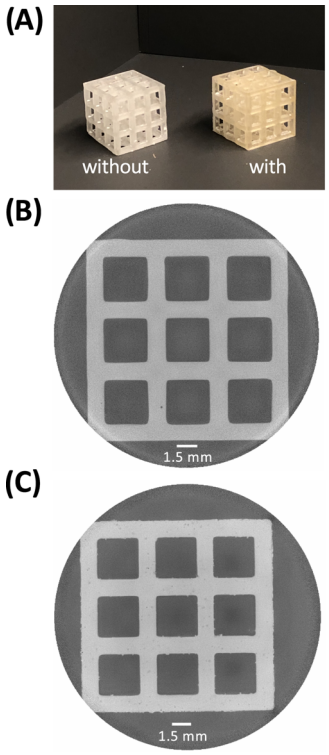

Figure 8. (A) Photograph of 15 × 15 × 15 mm^3 SLA 3D-printed grid lattice structures (left) without and (right) with EPA-filled microcapsules. Representative 2D slices from the 3D X-ray Nano-CT data for specimens (B) without capsules and (C) with capsules. See the Supporting Information for enlarged versions of X-ray Nano-CT images.

Table 2. Storage Modulus and Glass-Transition Temperature of SLA 3D-Printed Composites

microcapsule content (% w/w)	E' (MPa)	T_g (°C)
0	389 ± 14	62 ± 4
5	354 ± 18	61 ± 2

change in E' and T_g of SLA composites in the presence of capsules, mean and standard deviation of all values of both E' and T_g were determined to find the coefficient of variance (CV) across all measurements. CV was calculated as the ratio of standard deviation to mean, thereby representing the extent of variation in relation to the mean. The CVs for E' and T_g are 0.067 and 0.066, respectively. The CVs for both the storage modulus and T_g are less than 0.1 (10%), which is a typical metric for denoting a negligible difference between values.[52] These low standard deviations and CVs indicate low spread of data such that the addition of microcapsules and catalyst resulted in a negligible change in these physical properties of the SLA-printed composites.

3.3.2. Self-Healing Efficiency of SLA 3D-Printed Composites. The healing efficiencies of specimens with 5 wt % sieved DCPD-containing microcapsules and 0.5 wt % of catalyst were determined via the single-edge notch beam (SENB) fracture test. SENB fracture toughness tests provide an accurate protocol for investigating fracture behavior and healing efficiency of SLA-printed self-healing composites. After the fracture event, specimens were allowed to heal at room temperature for 24 and 72 h. These times were chosen to allow sufficient time for the healing and are commonly used temporal metrics in the literature for self-healing materials.[46−48] However, upon preliminary SENB testing, it was difficult to control the length of the propagated crack of these photocured composites after the fracture event (Supporting Information Figure S5), which tended to result in continued crack propagation through the width of the specimen. As the SENB test requires control over the initial crack length to target an approximate a/W value, this behavior prevents the use of this test method for evaluating healing efficiency. To alleviate this issue, a fracture relief defect (small hole of area 7.06 mm^2) was incorporated into the specimen to control the initial crack length and extract accurate fracture toughness from the SENB tests (Table 3).

When first comparing the fracture toughness of the initial samples, a 27% decrease in virgin fracture toughness and larger standard deviation was observed for the microcapsule-containing specimens compared to the specimens without microcapsules. Here, the spread was larger (especially for the microcapsule-containing specimens); however, the resulting standard deviation ranges of the measured fracture toughness for these 3D-printed specimens do overlap considerably. As observed with other composites, the microcapsules could be acting as defects in the polymer matrix, thus affecting fracture toughness.[49,50] However, material healing was obtained for the microcapsule-containing specimens at both 24 and 72 h with 53 and 73% of the prehealing fracture toughness recovered after healing, respectively. For the 3D-printed specimen, optical images of the crack developed after the fracture test, and its healing at 24 and 72 h, were obtained (Figure 9), which clearly show the initial healing of the fracture within 24 h and complete sealing of the fracture at 72 h. The increased healing efficiency with time is consistent with the literature on related self-healing materials,[25,53,54] and this dependence is mainly a consequence of the diffusion of polymer chains.[53] In future studies, other strategies including microcapsule loading and manipulating microcapsule size distributions will be investigated toward further increasing the healing efficiency and prehealing fracture toughness of these SLA 3D-printed composites.

4. CONCLUSIONS

In this work, we synthesized double-walled microcapsules encapsulating DCPD for incorporation in SLA 3D-printed materials. This is a versatile platform for SLA 3D printing of self-healing thermoset materials as it does not require manipulation of the resin chemistry and has less reliance on

Table 3. Fracture Toughness before and after Healing of Photocured Composites after 24 and 72 h

		24 h		72 h	
capsule loading (wt %)	prehealing fracture toughness ($MPa.m^{1/2}$)	posthealing fracture toughness ($MPa.m^{1/2}$)	self-healing efficiency (%)	posthealing fracture toughness ($MPa.m^{1/2}$)	self-healing efficiency (%)
0	719 ± 80				
5	524 ± 180	279 ± 68	53	384 ± 92	73

https://dx.doi.org/10.1021/acsapm.0c00872
ACS Appl. Polym. Mater. 2020, 2, 5048−5057

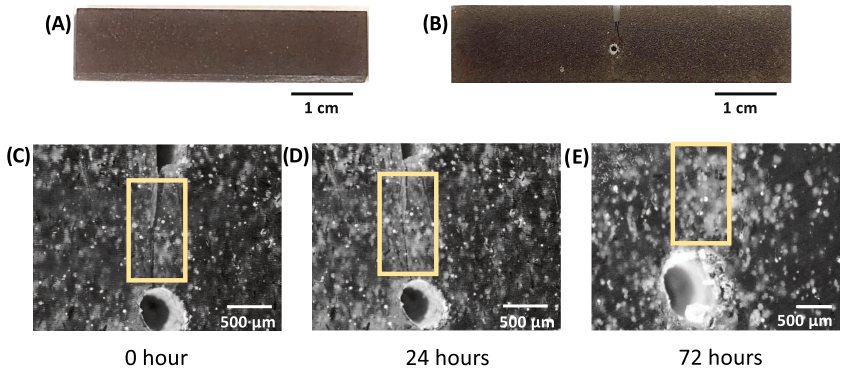

Figure 9. (A) 3D-printed composite structure containing DCPD-filled microcapsules and Grubbs' catalyst, (B) prenotched and precracked 3D-printed composite structure with a fracture relief defect, (C) optical microscopic images of prenotched and precracked composite, (D) and their crack healing in the photocured self-healing composite after 24 h and (E) 72 h.

compatibility with the healing fluid than a solvent healing-based microcapsule approach. The SLA 3D printing of commercial resin incorporating these self-healing microcapsules where the microcapsules remain intact after printing is demonstrated. X-ray Nano-CT imaging confirms an essentially uniform distribution of microcapsules within SLA 3D-printed cubes. This is desirable for self-healing composites to ensure that a given fracture will trigger self-healing through interaction with embedded microcapsules. Self-healing efficiency was investigated using SENB tests where a healing efficiency of 73% was achieved within 72 h of fracture. The ability of the DCPD monomer to polymerize in the presence of catalyst after a fracture event at room temperature without external stimulus is an important consideration for application of these systems. This study provides a platform for extending material lifetimes of 3D-printed materials via self-healing for recovery of structural integrity.

■ ASSOCIATED CONTENT

Supporting Information

The Supporting Information is available free of charge at https://pubs.acs.org/doi/10.1021/acsapm.0c00872.

Video of X-ray Nano-CT image stack edge for sample without microcapsules (AVI)

Video of X-ray Nano-CT image stack edge for sample with microcapsules (AVI)

Size distribution of EPA-filled microcapsules, DMA data, optical microscopy images of brittle fracture, and enlarged X-ray Nano-CT image (PDF)

■ AUTHOR INFORMATION

Corresponding Author

Bryan S. Beckingham − *Department of Chemical Engineering, Auburn University, Auburn, Alabama 36849, United States;* orcid.org/0000-0003-4004-0755; Phone: +1 (334) 844-2036; Email: bsb0025@auburn.edu

Authors

Vinita V. Shinde − *Department of Chemical Engineering, Auburn University, Auburn, Alabama 36849, United States*

Asha-Dee Celestine − *Department of Aerospace Engineering, Auburn University, Auburn, Alabama 36849, United States*

Lauren E. Beckingham − *Department of Civil and Environmental Engineering, Auburn University, Auburn, Alabama 36849, United States;* orcid.org/0000-0002-8433-9532

Complete contact information is available at: https://pubs.acs.org/10.1021/acsapm.0c00872

Author Contributions

The manuscript was written through the contribution of all authors. All authors have given approval to the final version of the manuscript.

Notes

The authors declare no competing financial interest.

■ ACKNOWLEDGMENTS

The authors acknowledge support from Gary Scheiffele and the University of Florida Research Service Centers for X-ray Nano-CT imaging of solid cubes. X-ray Nano-CT images of grid lattice structures were collected at Auburn University on a CT supported by the National Science Foundation under Grant No. 1919818. B.S.B., V.V.S., and A.-D.C. acknowledge financial support from the Auburn University Intramural Grants Program. This paper reflects the views and positions of the authors.

■ REFERENCES

(1) Schimpf, V.; Asmacher, A.; Fuchs, A.; Bruchmann, B.; Mülhaupt, R. Polyfunctional Acrylic Non-isocyanate Hydroxyurethanes as Photocurable Thermosets for 3D Printing. *Macromolecules* **2019**, *52*, 3288−3297.

(2) Tofail, S.; Koumoulos, E.; Bandyopadhyay, A.; Bose, S.; O'Donoghue, L.; Charitidis, C. Additive manufacturing: scientific and technological challenges, market uptake and opportunities. *Mater. Today* **2018**, *21*, 22−37.

(3) Hegde, M.; Meenakshisundaram, V.; Chartrain, N.; Sekhar, S.; Tafti, D.; Williams, C.; Long, T. 3D Printing All-Aromatic Polyimides using Mask-Projection Stereolithography: Processing the Non-processable. *Adv. Mater.* **2017**, *29*, No. 1701240.

(4) Zhao, Z.; Peng, F.; Cavicchi, K.; Cakmak, M.; Weiss, R.; Vogt, B. Three-Dimensional Printed Shape Memory Objects Based on an Olefin Ionomer of Zinc-Neutralized Poly(ethylene-co-methacrylic acid). *ACS Appl. Mater. Interfaces* **2017**, *9*, 27239−27249.

(5) Shi, Q.; Yu, K.; Kuang, X.; Mu, X.; Dunn, C.; Dunn, M.; Wang, T.; Qi, H. Recyclable 3D printing of vitrimer epoxy. *Mater. Horiz.* **2017**, *4*, 598−607.

(6) El Moumen, A.; Tarfaoui, M.; Lafdi, K. Additive manufacturing of polymer composites: Processing and modeling approaches. *Composites, Part B* **2019**, *171*, 166−182.

(7) Gebhardt, A.; Hotter, J. Additive Manufacturing. 2016, pp 97−107.
(8) Arnold, C.; Monsees, D.; Hey, J.; Schweyen, R. Surface Quality of 3D-Printed Models as a Function of Various Printing Parameters. *Materials* **2019**, *12*, 1970.
(9) Singh, R.; Zhang, M.; Chan, D. Toughening of a brittle thermosetting polymer: Effects of reinforcement particle size and volume fraction. *J. Mater. Sci.* **2002**, *37*, 781−788.
(10) Sultan, J.; McGarry, F. Effect of rubber particle size on deformation mechanisms in glassy epoxy. *Polym.Eng. Sci.* **1973**, *13*, 29−34.
(11) Manzione, L.; Gillham, J.; McPherson, C. Rubber-modified epoxies. II. Morphology and mechanical properties. *J. Appl. Polym. Sci.* **1981**, *26*, 907−919.
(12) Yee, A.; Pearson, R. Toughening mechanisms in elastomer-modified epoxies: Part 1 Mechanical studies. *J. Mater. Sci.* **1986**, *21*, 2462−2474.
(13) Toohey, K.; Sottos, N.; Lewis, J.; Moore, J.; White, S. Self-healing materials with microvascular networks. *Nat. Mater.* **2007**, *6*, 581−585.
(14) Amstad, E. Capsules: Their Past and Opportunities for Their Future. *ACS Macro Lett.* **2017**, *6*, 841−847.
(15) Bekas, D.; Tsirka, K.; Baltzis, D.; Paipetis, A. Self-healing materials: A review of advances in materials, evaluation, characterization and monitoring techniques. *Composites, Part B* **2016**, *87*, 92−119.
(16) Blaiszik, B.; Kramer, S.; Olugebefola, S.; Moore, J.; Sottos, N.; White, S. Self-Healing Polymers and Composites. *Annu. Rev. Mater. Res.* **2010**, *40*, 179−211.
(17) Wang, Z.; Lu, X.; Sun, S.; Yu, C.; Xia, H. Preparation, characterization and properties of intrinsic self-healing elastomers. *J. Mater. Chem. B* **2019**, *7*, 4876−4926.
(18) Hayes, S.; Swait, T.; Lafferty, A. *Recent Advances in Smart Self-healing Polymers and Composites*; Elsevier, 2015; pp 162−165.
(19) Yang, Y.; Lu, X.; Wang, W. A tough polyurethane elastomer with self-healing ability. *Mater. Des.* **2017**, *127*, 30−36.
(20) Gladman, A.; Celestine, A.; Sottos, N.; White, S. Autonomic Healing of Acrylic Bone Cement. *Adv. Healthcare Mater.* **2015**, *4*, 202−207.
(21) White, S.; Sottos, N.; Geubelle, P.; Moore, J.; Kessler, M.; Sriram, S.; Brown, E.; Viswanathan, S. Autonomic healing of polymer composites. *Nature* **2001**, *409*, No. 794.
(22) Caruso, M.; Blaiszik, B.; Jin, H.; Schelkopf, S.; Stradley, D.; Sottos, N.; White, S.; Moore, J. Robust, Double-Walled Microcapsules for Self-Healing Polymeric Materials. *ACS Appl. Mater. Interfaces* **2010**, *2*, 1195−1199.
(23) Jones, A.; Watkins, C.; White, S.; Sottos, N. Self-healing thermoplastic-toughened epoxy. *Polymer* **2015**, *74*, 254−261.
(24) Sanders, P.; Young, A.; Qin, Y.; Fancey, K.; Reithofer, M.; Guillet-Nicolas, R.; Kleitz, F.; Pamme, N.; Chin, J. Stereolithographic 3D printing of extrinsically self-healing composites. *Sci. Rep.* **2019**, *9*, No. 388.
(25) Celestine, A.; Sottos, N.; White, S. Autonomic healing of PMMA via microencapsulated solvent. *Polymer* **2015**, *69*, 241−248.
(26) Brochu, A. B. W.; Evans, G.; Reichert, W. Mechanical and cytotoxicity testing of acrylic bone cement embedded with microencapsulated 2-octyl cyanoacrylate. *J. Biomed. Mater. Res., Part B* **2014**, *102*, 181−189.
(27) Jones, A.; Watkins, C.; White, S.; Sottos, N. Self-healing thermoplastic-toughened epoxy. *Polymer* **2015**, *74*, 254−261.
(28) Szabó, T.; Telegdi, J.; Nyikos, L. Linseed oil-filled microcapsules containing drier and corrosion inhibitor − Their effects on self-healing capability of paints. *Prog. Org. Coat.* **2015**, *84*, 136−142.
(29) Behzadnasab, M.; Esfandeh, M.; Mirabedini, S.; Zohuriaan-Mehr, M.; Farnood, R. Preparation and characterization of linseed oil-filled urea−formaldehyde microcapsules and their effect on mechanical properties of an epoxy-based coating. *Colloids Surf., A.* **2014**, *457*, 16−26.
(30) Greenland, B.; Hayes, W.; et al. Healable supramolecular polymers. *Polym. Chem.* **2013**, *4*, 4860.
(31) Blaiszik, B.; Baginska, M.; White, S.; Sottos, N. Autonomic Recovery of Fiber/Matrix Interfacial Bond Strength in a Model composite. *Adv. Funct. Mater.* **2010**, *20*, 3547−3554.
(32) Uzcategui, A.; Muralidharan, A.; Ferguson, V.; Bryant, S.; McLeod, R. Understanding and Improving Mechanical Properties in 3D printed Parts Using a Dual-Cure Acrylate-Based Resin for Stereolithography. *Adv. Eng. Mater.* **2018**, *20*, No. 1800876.
(33) Dizon, J.; Espera, A.; Chen, Q.; Advincula, R. Mechanical characterization of 3D-printed polymers. *Addit. Manuf.* **2018**, *20*, 44−67.
(34) Postiglione, G.; Alberini, M.; Leigh, S.; Levi, M.; Turri, S. Effect of 3D-printed microvascular network design on the self-healing behaviour of crosslinked polymers. *ACS Appl. Mater. Interfaces* **2017**, *9*, 14371−14378.
(35) Deng, X.; Attalla, R.; Sadowski, L. P.; Chen, M.; Majcher, M. J.; Urosev, I.; Yin, D.-C.; Selvaganapathy, P. R.; Filipe, C. D. M.; Hoare, T. Autonomously Self-Adhesive Hydrogels as Building Blocks for Additive Manufacturing. *Biomacromolecules* **2018**, *19*, 62−70.
(36) Almutairi, M.; Aria, A.; Thakur, V.; Khan, M. Self-Healing Mechanisms for 3D-Printed Polymeric Structures: From Lab to Reality. *Polymers* **2020**, *12*, No. 1534.
(37) Yu, K.; Xin, A.; Du, H.; Li, Y.; Wang, Q. Additive manufacturing of self-healing elastomers. *NPG Asia Mater.* **2019**, *11*, No. 7.
(38) Liu, S.; Li, L. Ultra-stretchable and Self-healing Double Network Hydrogel for 3D Printing and Strain Sensor. *ACS Appl. Mater. Interfaces* **2017**, *9*, 26429−26437.
(39) Nadgorny, M.; Xiao, Z.; Connal, L. 2D and 3D-printing of self-healing gels: design and extrusion of self-rolling objects. *Mol. Syst. Des. Eng.* **2017**, *2*, 283−292.
(40) Highley, C.; Rodell, C.; Burdick, J. Direct 3D Printing of Shear-Thinning Hydrogels into Self-Healing Hydrogels. *Adv. Mater.* **2015**, *27*, 5075−5079.
(41) Jang, T. S.; Jung, H.; Pan, H.; Han, W.; Chen, S.; Song, J. 3D printing of hydrogel composite systems: Recent advances in technology for tissue engineering. *Int. J. Bioprint.* **2018**, *4*, No. 126.
(42) Neuser, S.; Michaud, V. Fatigue Response of Solvent-Based Self-Healing Smart Materials. *Exp. Mech.* **2014**, *54*, 293−304.
(43) Postiglione, G.; Turri, S.; Levi, M. Effect of the Plasticizer on the Self-Healing Properties of a Polymer Coating Based on the Thermoreversible Diels−Alder Reaction. *Prog. Org. Coat.* **2015**, *78*, 526−531.
(44) Wu, D. Y.; Meure, S.; Solomon, D. Self-Healing Polymeric Materials: a Review of Recent Developments. *Prog. Polym. Sci.* **2008**, *33*, 479−522.
(45) Sharma, A.; Pandey, A.; Shukla, D.; Pandey, K. Effect of Self-Healing Dicyclopentadiene Microcapsules on Fracture Toughness of Epoxy. *Mater. Today: Proc.* **2018**, *5*, 21256−21262.
(46) Patrick, J.; Sottos, N.; White, S. Microvascular based self-healing polymeric foam. *Polymer* **2012**, *53*, 4231−4240.
(47) Crespy, D.; Landfester, K.; Fickert, J.; Rohwerder, M. Advances in Polymer Science Series 2016, Vol. *273*, pp 247−283.
(48) Aniskevich, A.; Kulakov, V.; Bulderberga, O.; Knotek, P.; Tedim, J.; Maia, F.; Leisis, V.; Zeleniakiene, D. Experimental characterisation and modelling of mechanical behaviour of microcapsules. *J. Mater. Sci.* **2020**, *55*, 13457−13471.
(49) Brown, E.; White, S.; Sottos, N. Microcapsule induced toughening in a self-healing polymer composite. *J. Mater. Sci.* **2004**, *39*, 1703−1710.
(50) Albdiry, M.; Yousif, B. Toughening of brittle polyester with functionalized halloysite nanocomposites. *Composites, Part B* **2019**, *160*, 94−109.
(51) Yang, C.; Huh, H.; Hahn, H. Investigation of effective material properties in composites with internal defect or reinforcement particles. *Int. J. Solids Struct.* **2005**, *42*, 6141−6165.

https://dx.doi.org/10.1021/acsapm.0c00872
ACS Appl. Polym. Mater. 2020, 2, 5048−5057

(52) Romano, F.; Ambrosano, G.; Magnani, M.; Nouer, D. Analysis of the coefficient of variation in shear and tensile bond strength tests. *J. Appl. Oral Sci.* **2005**, *13*, 243−246.
(53) Wool, R.; O'Connor, K. A theory crack healing in polymers. *J. Appl. Phys.* **1981**, *52*, 5953−5963.
(54) Jud, K.; Kausch, H. Load transfer through chain molecules after interpenetration at interfaces. *Polym. Bull.* **1979**, *1*, 697−707.

https://dx.doi.org/10.1021/acsapm.0c00872
ACS Appl. Polym. Mater. 2020, 2, 5048−5057